Object-oriented Modeling for Planning and Control of Multi-energy Systems

Stefan Bschorer, Maren Kuschke, and Kai Strunz

Abstract—**Multi-energy systems (MES) involving networks of different energy carriers can support the balancing of fluctuating renewable generation by co-ordinated joint operation. In this paper, an object-oriented modeling methodology for planning and operations control of MES based on nodal analysis is proposed. The framework provides the modularity to simulate scenarios with varying network configurations. Based on object-oriented programming, classes are formed with regard to common attributes of the network elements. The instances of classes represent physical network elements, such as buses, lines, and power conversion units. The models of the individual network elements involve adjustable and flexible parameters. This is especially advantageous for scenarios with operating-point-dependent efficiencies. The overall framework makes use of a uniform description of the model parameters across the diverse energy carriers. Thus, the methodology is particularly suited for the analysis of MES. The applicability of the modeling framework is demonstrated by two use cases involving a technology campus in Berlin.**

Index Terms—**Control of multi-energy systems, cooling network, demand-side management, electric network, heating network, object-oriented programming, operations control of multi-energy systems, planning of multi-energy systems, smart grids.**

I. Introduction

MULTI-energy systems (MES) can provide increased flexibility for the integration of volatile renewable power generators, such as wind turbines and photovoltaics, into the electric power system. In MES, the electric part of the power system benefits from available flexibility in networks of other energy carriers [1], [2]. Those networks are connected to the electric power system by power conversion units. These units can be controlled to adapt themselves to the output from renewable resources, making use of available flexible demand and storage capacity in the networks of other energy carriers [3]. An example of an MES with electricity, heating, and cooling networks is illustrated in Fig. 1. There, the combined heat and power unit (CHP) as well as battery, heat, and cold storage units are controlled by an energy management system performing operations control. Thus, the generation from local photovoltaics as well as wind and solar farms can be balanced.

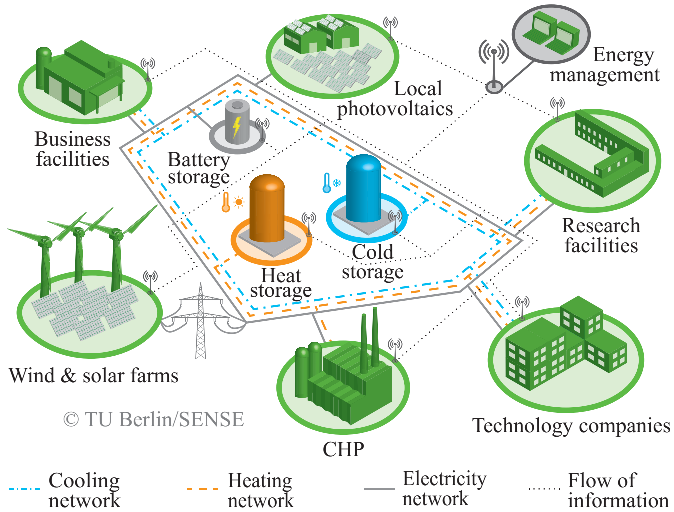

Fig. 1. Illustration of a multi-energy system.

For the operations control of the entire MES, an adequate model of the participating energy carrier networks and resources, with special regard to controllable conversion units, storage units, and prosumers, is essential. In the literature, different approaches are proposed. In [4]–[6], combined cooling, heating, and electric power systems are analyzed while disregarding network connections. Therefore, the positioning of individual units cannot be studied. One approach considering network connections is the energy hub concept of [7]. In energy hubs, storage and conversion of multiple energy carriers take place. As described in [8], network connections are realized by linking several hubs. In [9], this concept is applied to the connection of electricity and heating networks of several facilities modeled as hubs. In [10], an algorithm is proposed to identify the optimal configuration of electricity and gas networks, adapting links between hubs.

In an energy hub, controllable power conversion and energy storage units are clustered. The clustering is automated by [11] and [12] to face changes in the composition of hubs more efficiently. The approach in [13] addresses the optimal clustering. Due to the clustering, only the total power of each carrier per energy hub is determined. Therefore, the contribution of individual units cannot be identified. According to [14], the

Manuscript received March 25, 2019; revised May 23, 2019; accepted June 11, 2019. Date of publication September 30, 2019; date of current version August 16, 2019. This work was supported by the project "Energienetz Berlin Adlershof" (no. 03ET1038G), funded by the German Federal Ministry of Economic Affairs and Energy (BMWi).

S. Bschorer (corresponding author, email: stefan.bschorer@tu-berlin.de), M. Kuschke and K. Strunz are with the Chair of Sustainable Electric Networks and Sources of Energy, School of Electrical Engineering and Computer Science, Technische Universität Berlin, 10623 Berlin, Germany.

DOI: 10.17775/CSEEJPES.2019.00650

definition of sub hubs inside an energy hub allows for the analysis of individual units. With only one sub hub per energy carrier summing up the power of all related units, network connections are not modeled.

In contrast to the aforementioned approaches, network connections within an energy hub are facilitated by the concept in [15] based on graph theory. This concept has shown to be effective for control applications such as demand-side management. In the control application, power conversion parameters are modeled with constant efficiencies. However, for certain tasks of planning and control of MES, the representation of power conversion processes with operating-point-dependent efficiencies may be critical. This is of importance for the application cases considered in the present work.

In this paper, an object-oriented modeling approach based on nodal analysis for planning and operations control of MES is proposed. The following features are covered:

1) The presented object-oriented structure defines base classes representing an MES. This framework provides modularity and expandability.
2) Thanks to the abstraction of formulating classes that are representative of diverse energy carriers, the approach is well-suited for modeling of MES.
3) In analogy to nodal analysis, network power balances are realized by node objects. The nodal analysis technique supports arbitrary and flexible network topologies.
4) The instances of the classes find their counterparts in physical network elements, such as network buses, lines, and power conversion units. This enables the analysis of particular units with adjustable and flexible parameters.
5) The object-oriented approach is applied to two use cases demonstrating the applicability for planning and control of MES. Both application cases pertain to the high-technology campus Berlin-Adlershof.

Following this introduction, the design of the modeling framework is proposed in Section II. The application of the object-oriented programming approach and the integration of the model into the optimization framework are described. In preparation for the case studies, Section III provides models of selected resources. In Section IV, two case studies put into evidence the applicability of the developed object-oriented modeling approach. Conclusions are drawn in Section V.

II. Object-oriented Modeling Framework

In accordance with object-oriented programming [16], categories of network elements are formed. The categories constitute the classes with regard to common attributes and functions. Representing an MES, the three classes "Node", "Branch", and "Resource" are defined. The role of the class "Node" is to ensure power balance. This is in analogy to Kirchhoff's current law, where at each electrical node the currents are summed up to zero. Allocated network elements for power transfer and intra-carrier power conversion, i.e. a power conversion process where input and output concern one and the same energy carrier, are defined by class "Branch". Inter-carrier power conversion units, energy storage units, and prosumers belong to class "Resource". In the following Subsection II-A the proposed specification of the classes is presented. Details of the integration into the optimization framework are provided in Subsection II-B.

A. Specification of Classes

The class "Node" represents network nodes, such as buses, junctions, and manifolds, as presented in Table I. Each node object $\mathrm{No}_{i,\alpha}$ is identified by node number i and energy carrier α. Number i is an element of the set of all node numbers $\mathcal{I} \subset \mathbb{N}$, energy carrier α is an element of the set of all energy

TABLE I
SPECIFICATION OF CLASSES

Class name		Node	Branch	Resource
Illustration		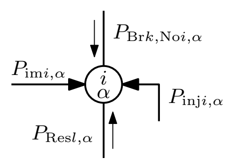	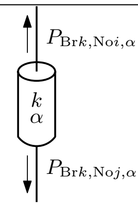	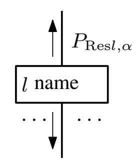
Represented network elements		Network buses, junctions, and manifolds	Network lines and pipes, Intra-carrier power conversion units	Inter-carrier power conversion units, Energy storage units, Prosumers
Attributes	Identifier	Node number $i \in \mathcal{I} \subset \mathbb{N}$ Energy carrier $\alpha \in \mathcal{C}$	Branch number $k \in \mathcal{K} \subset \mathbb{N}$ Energy carrier $\alpha \in \mathcal{C}$	Resource number $l \in \mathcal{L} \subset \mathbb{N}$ Resource name
	Allocations	Identifiers of allocated branches $\mathrm{Br}_{k,\alpha}\quad \forall k \in \mathcal{K}_i$ Identifiers of allocated resources $\mathrm{Res}_l \quad \forall l \in \mathcal{L}_i$	Identifiers of the two allocated nodes $\mathrm{No}_{i,\alpha}$ and $\mathrm{No}_{j,\alpha}$ with $i, j \in \mathcal{I}_k$	Identifiers of allocated nodes $\mathrm{No}_{i,\alpha} \quad \forall i \in \mathcal{I}_l$ and for $\alpha \in \mathcal{C}$
	Operation parameter vectors	Uncontrollable nodal power injection $\boldsymbol{P}_{\mathrm{inj}i,\alpha}$ Limits of power import $\boldsymbol{P}^{\min}_{\mathrm{im}i,\alpha}$, $\boldsymbol{P}^{\max}_{\mathrm{im}i,\alpha}$	Transfer efficiency $\boldsymbol{\eta}_{\mathrm{Br}k,\alpha}$ Limits of power transfer $\boldsymbol{P}^{\min}_{\mathrm{Br}k,\alpha}$, $\boldsymbol{P}^{\max}_{\mathrm{Br}k,\alpha}$	Depending on subclass
	Optimization variables	Power import $\boldsymbol{P}_{\mathrm{im}i,\alpha}$	Power at the beginning and at the end of the line $\boldsymbol{P}_{\mathrm{Br}k,\mathrm{No}i,\alpha}$, $\boldsymbol{P}_{\mathrm{Br}k,\mathrm{No}j,\alpha}$	Depending on subclass
Operations		Power balance	Power transfer	Depending on subclass

carriers $\mathcal{C}$. As nodes serve as coupling elements, the identifiers of the allocated branch objects $\mathrm{Br}_{k,\alpha}$ and resource objects Res_l are listed in the attributes of the class. Branch numbers $k \in \mathcal{K}_i$ indicate the branch objects allocated to $\mathrm{No}_{i,\alpha}$. Analogously, $l \in \mathcal{L}_i$ give the resource numbers of all resource objects allocated to $\mathrm{No}_{i,\alpha}$. The number of allocated objects is not limited.

The list of attributes of the node further contains operational parameters defining uncontrollable nodal power injection and limits of optimization variables. Nodal power injection $P_{\mathrm{inj}i,\alpha}$ represents uncontrollable demand and generation, such as lighting of household load or renewable power, and it is directly assigned to the node object. In addition, the power exchange with external networks of the same energy carrier is directly assigned. This power is represented by the optimization variable for power import $P_{\mathrm{im}i,\alpha}$. Negative values of $P_{\mathrm{im}i,\alpha}$ correspond to power export.

The net sum of power flows at each node object must equal zero. The class "Node" so contributes the power balance equation to the constraints of the optimization problem. The value of the power is positive if the physical direction of the flow coincides with the direction of the arrow as illustrated in Table I. Therefore, the power balance performed by node object $\mathrm{No}_{i,\alpha}$ at each time point t_n results in:

$$\begin{aligned} &P_{\mathrm{im}i,\alpha}(t_n) + P_{\mathrm{inj}i,\alpha}(t_n) \\ &+ \sum_{k\in\mathcal{K}_i} P_{\mathrm{Br}k,\mathrm{No}i,\alpha}(t_n) + \sum_{l\in\mathcal{L}_i} P_{\mathrm{Res}l,\alpha}(t_n) = 0 \end{aligned} \tag{1}$$

Parameter $P_{\mathrm{Br}k,\mathrm{No}i,\alpha}$ is a direct input from allocated objects of class "Branch". As given in Table I, this class represents lines and pipes as well as intra-carrier conversion units like transformers. Each branch object is identified by branch number $k \in \mathcal{K} \subset \mathbb{N}$ and energy carrier $\alpha \in \mathcal{C}$. As a branch object is allocated to exactly two node objects of the same energy carrier, the identifiers $\mathrm{No}_{i,\alpha}$ and $\mathrm{No}_{j,\alpha}$ are part of the branch attributes. Node numbers $i, j \in \mathcal{I}_k$ are the node numbers allocated to $\mathrm{Br}_{k,\alpha}$. The operation parameters of the branch object involve transfer efficiency $\eta_{\mathrm{Br}k,\alpha}$ and limits of power transfer. Considering the direction, the power transfer between $\mathrm{No}_{i,\alpha}$ and $\mathrm{No}_{j,\alpha}$ is given by:

$$\begin{aligned} &P_{\mathrm{Br}k,\mathrm{No}j,\alpha}(t_n) = \\ &\begin{cases} -\dfrac{1}{\eta_{\mathrm{Br}k,\alpha}} \cdot P_{\mathrm{Br}k,\mathrm{No}i,\alpha}(t_n), & P_{\mathrm{Br}k,\mathrm{No}i,\alpha}(t_n) \geq 0 \\ -\eta_{\mathrm{Br}k,\alpha} \cdot P_{\mathrm{Br}k,\mathrm{No}i,\alpha}(t_n), & P_{\mathrm{Br}i,\mathrm{No}i,\alpha}(t_n) < 0 \end{cases} \end{aligned} \tag{2}$$

The values of $P_{\mathrm{Br}k,\mathrm{No}i,\alpha}$ and $P_{\mathrm{Br}k,\mathrm{No}j,\alpha}$ are positive if the physical directions of the flows agree with the directions of the arrows as illustrated in Table I.

The class "Resource" represents controllable power conversion units, energy storage units, and prosumers. In accordance with Table I, resource objects Res_l are indicated by resource number $l \in \mathcal{L} \subset \mathbb{N}$ and by a resource name, which is freely selectable. Dependent on the type, resource objects are allocated to one or more node objects of different energy carriers. The identifiers of allocated node objects $\mathrm{No}_{i,\alpha}$ are listed in the attributes. Node numbers $i \in \mathcal{I}_l$ indicate the node objects allocated to Res_l.

As opposed to the classes "Node" and "Branch", the class "Resource" is an abstract class that has no instances. Operation parameters, optimization variables, and operations are defined in subclasses. Fig. 2 illustrates the class diagram according to the notation in [16]. Abstract classes are marked with an "A" inside a triangle. The class "Resource" inherits the subclasses "Inter-carrier conversion", "Storage", and "Prosumer". Instances of the latter refer to network elements, such as shiftable and interruptible demand. However, the other two classes again inherit two subclasses. The subclasses of class "Inter-carrier conversion" are "SISO conversion" and "SIDO conversion". SISO and SIDO signify "single-input single-output" and "single-input dual-output", respectively. This notation refers to the number of input and output nodes the conversion unit is allocated to. For example, class "SISO conversion" represents heat pumps and gas boilers, whereas conversion units such as CHP and compression chiller are modeled as objects of class "SIDO conversion". Class "Storage" inherits the subclasses "Single carrier storage" and "Dual carrier storage", which distinguish between the number of involved energy carriers. Most of the storage units, such as battery storage units, heat storage units, and cold storage units, are represented by class "Single carrier storage". An example for an instance of class "Dual carrier storage" is the ice storage unit, which is charged at a different temperature than it is discharged, involving transitions of phase.

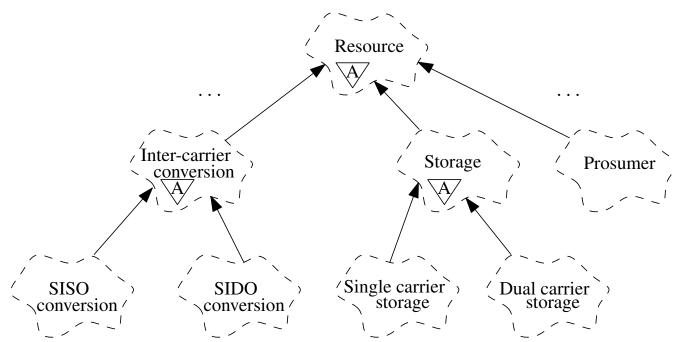

Fig. 2. Class diagram with subclasses of abstract class "Resource".

B. Integration into Optimization Framework

The developed modeling methodology can be integrated into an optimization framework for determining the optimal operation of the resources. The formulation of the optimization problem considering operational behavior and constraints of resources, such as nonlinear performance curves and power limits, results in a mixed integer nonlinear program. As a trade-off between computing time and modeling accuracy, nonlinear performance curves are linearized, as e.g. shown in [4]–[6]. Solving the optimization problem, mixed integer linear optimization programming (MILP) is applied. An MILP formulation with objective function (3), constraints (4), and bounds (5) is defined as:

$$\text{minimize} \quad f(\boldsymbol{x},\boldsymbol{y}) = \boldsymbol{c}^{\mathsf{T}}\boldsymbol{x} + \boldsymbol{d}^{\mathsf{T}}\boldsymbol{y} \tag{3}$$

$$\text{subject to} \quad \boldsymbol{A}\boldsymbol{x} + \boldsymbol{B}\boldsymbol{y} \geq \boldsymbol{b} \tag{4}$$

$$\boldsymbol{x} \geq \boldsymbol{0}, \boldsymbol{y} \geq \boldsymbol{0}, \tag{5}$$

TABLE II
SPECIFICATION OF SELECTED RESOURCES

Resource name		**Chiller**	**Ice storage**	**Shiftable demand**
Illustration		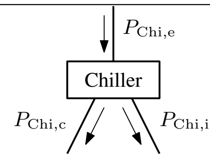	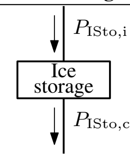	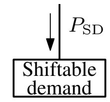
Instance of class		**SIDO conversion**	**Dual carrier storage**	**Prosumer**
Attributes	Allocations	Identifiers of allocated nodes $\mathrm{No}_{i,\mathrm{e}}$, $\mathrm{No}_{i,\mathrm{c}}$, $\mathrm{No}_{i,\mathrm{i}}$	Identifiers of allocated nodes $\mathrm{No}_{i,\mathrm{c}}$, $\mathrm{No}_{i,\mathrm{i}}$	Identifier of allocated node $\mathrm{No}_{i,\alpha}$
	Operation parameters	Nominal conversion efficiencies $\eta^{\mathrm{nom}}_{\mathrm{Chi,c}}$, $\eta^{\mathrm{nom}}_{\mathrm{Chi,i}}$ Nominal input power $P^{\mathrm{nom}}_{\mathrm{Chi,e}}$ Nominal output power $P^{\mathrm{nom}}_{\mathrm{Chi,c}}$, $P^{\mathrm{nom}}_{\mathrm{Chi,i}}$ Coefficients of load profiles $a_{\mathrm{c}}(\vartheta_{\mathrm{a}})$, $a_{\mathrm{i}}(\vartheta_{\mathrm{a}})$, $b_{\mathrm{c}}(\vartheta_{\mathrm{a}})$, $b_{\mathrm{i}}(\vartheta_{\mathrm{a}})$	Storage efficiencies $\eta_{\mathrm{ISto,cha}}$, $\eta_{\mathrm{ISto,dis}}$, $\eta_{\mathrm{ISto,sd}}$ Maximum charging and discharging power $P^{\mathrm{max}}_{\mathrm{Isto,i}}$, $P^{\mathrm{max}}_{\mathrm{Isto,c}}$ Storage capacity limits $E^{\mathrm{min}}_{\mathrm{Isto}}$, $E^{\mathrm{max}}_{\mathrm{Isto}}$ Initial and final energy level $E^{\mathrm{ini}}_{\mathrm{ISto}}$, $E^{\mathrm{end}}_{\mathrm{ISto}}$	Planned power demand $\boldsymbol{P}_{\mathrm{SD,plan}}$ Original starting time t_o Maximum time shift Δt_s
	Optimization variables	Input power $\boldsymbol{P}_{\mathrm{Chi,e}}$ Output power $\boldsymbol{P}_{\mathrm{Chi,c}}$, $\boldsymbol{P}_{\mathrm{Chi,i}}$	Charging and discharging power $\boldsymbol{P}_{\mathrm{Isto,i}}$, $\boldsymbol{P}_{\mathrm{Isto,c}}$ Energy level $\boldsymbol{E}_{\mathrm{ISto}}$	Shifted power demand $\boldsymbol{P}_{\mathrm{SD}}$
Operations		Power conversion	Energy storage	Demand-side management

where $\boldsymbol{x} \in \mathbb{R}^n$ and $\boldsymbol{y} \in \mathbb{Z}^p$ denote, respectively, the n-dimensional vector of continuous variables and the p-dimensional vector of integer variables. Furthermore, $\boldsymbol{c} \in \mathbb{R}^n$ and $\boldsymbol{d} \in \mathbb{R}^p$ are the vectors of objective coefficients, $\boldsymbol{b} \in \mathbb{R}^m$ is the vector of coefficients of the m constraints, and $\boldsymbol{A} \in \mathbb{R}^{m\times n}$ and $\boldsymbol{B} \in \mathbb{R}^{m\times p}$ are the matrices of constraints with real coefficients of dimensions $(m \times n)$ and $(m \times p)$, respectively.

The optimization problem is formulated in linear programming (LP) format, fitting the requirements of the most common MILP based solvers. The objective function and the objective coefficients depend on the application case. Constraints and bounds for power balance, power transfer, as well as power conversion, energy storage, and prosumer operation are set up by specific objects.

III. MODELING OF SELECTED RESOURCES

The class "Resource" inherits the three subclasses "Inter-carrier conversion", "Storage", and "Prosumer". In preparation for the application cases in Section IV, three models of different subclasses are presented. Besides compression chiller and ice storage unit, shiftable demand is modeled. With regard to the compression chiller, the originally non-linear performance curves are approximated by piecewise linear profiles. The ice storage unit is allocated to two nodes, taking into consideration the different energy carriers at charging and discharging. As an example for a prosumer, a model for shiftable demand is provided. The operation parameters and optimization variables of the selected resources are summarized in Table II.

A. Compression Chiller

A compression chiller converts electric power to cooling power operating on a vapor-compression cycle [17]. As presented in [18], the electric power consumption depends on cooling demand, ambient temperature, and flow temperature. The chiller considered here can switch between two operating modes. In mode "cooling", the temperature of the refrigerant is +4°C. In mode "ice", an ice storage unit is charged, and the refrigerant is cooled down to −5°C.

The relation of electric power and cooling power can be modeled by different approaches [19]–[21]. Here, a linear regression model as presented in [20] is applied. The piecewise linear model is parametrized based on data sheet [22] and measurements. The resulting piecewise linear load profiles are presented in Fig. 3 for selected ambient temperatures and for both operating modes. The chiller is designed to generate 1 pu of cooling power $P_{\mathrm{Chi,c}}$ and to consume 1 pu of electric power $P_{\mathrm{Chi,e}}$ at an ambient temperature of 35°C. As the chiller operates more efficiently at lower ambient temperatures, $P_{\mathrm{Chi,c}}$ may exceed 1 pu. According to [18], $P_{\mathrm{Chi,e}}$ is related to $P_{\mathrm{Chi,c}}$ and $P_{\mathrm{Chi,i}}$, respectively, as follows:

$$P_{\mathrm{Chi,e}}(t_n) = \begin{cases} a_{\mathrm{c}}(\vartheta_{\mathrm{a}}(t_n)) \cdot P_{\mathrm{Chi,c}}(t_n) + b_{\mathrm{c}}(\vartheta_{\mathrm{a}}(t_n)), & \text{mode "cooling"} \\ a_{\mathrm{i}}(\vartheta_{\mathrm{a}}(t_n)) \cdot P_{\mathrm{Chi,i}}(t_n) + b_{\mathrm{i}}(\vartheta_{\mathrm{a}}(t_n)), & \text{mode "ice"} \end{cases} \tag{6}$$

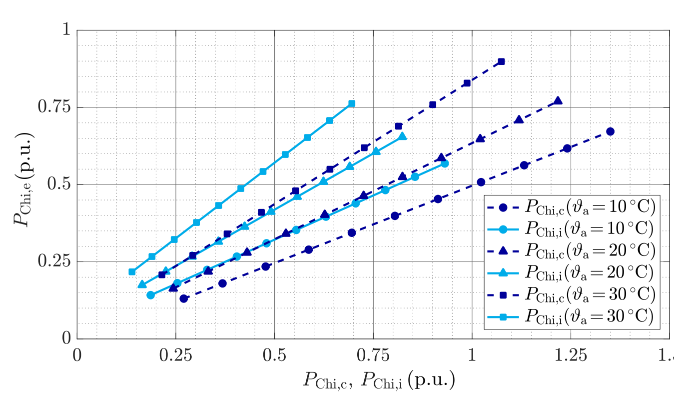

Fig. 3. Piecewise linear load profiles of a compression chiller.

The parameters a_{c} and a_{i} determine the slope, and b_{c} and b_{i} determine the y-intercept of the load profiles. These parameters are dependent on the ambient temperature ϑ_{a}. According to the illustration in Table II, the values of input and output power are positive. To account for the operating modes, the chiller is allocated to an electricity node $\mathrm{No}_{i,\mathrm{e}}$, a cooling node $\mathrm{No}_{i,\mathrm{c}}$, and an ice node $\mathrm{No}_{i,\mathrm{i}}$. As there are one input and two output nodes, the presented chiller is of class "SIDO conversion".

B. Ice Storage Unit

An ice storage unit uses the latent heat of fusion of water of 335 kJ/kg to store cooling energy [23]. Therefore, the energy density of an ice storage unit is higher than the energy density of a sensible cooling storage unit. An ice storage unit in a cooling system is charged by a flow of a temperature below 0°C and discharged by a return fluid of higher temperatures from the cooling network. Thus, the ice storage is allocated to a node of energy carrier "ice" as well as to a node of energy carrier "cooling". Therefore, the ice storage unit is modeled as a representative of the subclass "Dual carrier storage". Considering the efficiencies at charging $\eta_{\mathrm{ISto,cha}}$ and discharging $\eta_{\mathrm{ISto,dis}}$ as well as the self-discharge efficiency $\eta_{\mathrm{ISto,sd}}$, the energy level E_{ISto} is determined as:

$$E_{\mathrm{ISto}}(t_n) = \eta_{\mathrm{ISto,sd}} \cdot E_{\mathrm{ISto}}(t_{n-1}) + \eta_{\mathrm{ISto,cha}} \cdot P_{\mathrm{ISto,i}}(t_n) \cdot \tau - \frac{1}{\eta_{\mathrm{ISto,dis}}} \cdot P_{\mathrm{ISto,c}}(t_n) \cdot \tau \tag{7}$$

where τ is the time step size. Charging power $P_{\mathrm{ISto,i}}$ and discharging power $P_{\mathrm{ISto,c}}$ are positive values.

C. Shiftable Demand

Shiftable demand is modeled as an object of class "Prosumer". Following [24], the shiftable demand is defined as the planned daily demand profile vector $\boldsymbol{P}_{\mathrm{SD,plan}} \in \mathbb{R}^r$ which can be shifted forward and backward in time. Index r indicates the number of time points within a day. The set of all possibilities of shifted load profiles is stored in the matrix $\boldsymbol{P}_{\mathrm{set}} \in \mathbb{R}^{r\times(s+1)}$. Each column represents one option. The number of options $(s+1)$ depends on the maximum time shift Δt_s. The shifted power demand $\boldsymbol{P}_{\mathrm{SD}} \in \mathbb{R}^r$ after shifting is determined by:

$$\boldsymbol{P}_{\mathrm{SD}} = \boldsymbol{P}_{\mathrm{set}}\boldsymbol{y}_{\mathrm{SD}} \tag{8}$$

where $\boldsymbol{y}_{\mathrm{SD}} \in \{0,1\}^{(s+1)\times 1}$ identifies the column of $\boldsymbol{P}_{\mathrm{set}}$ with the resulting shifted demand profile. There is only one nonzero element in $\boldsymbol{y}_{\mathrm{SD}}$ which is equal to one.

IV. Application and Validation

In the following, two study cases to validate the applicability of the methodology are presented. Both applications refer to Berlin-Adlershof, one of the most successful high-technology campus sites in Germany.

Case 1 demonstrates how the object-oriented modeling approach is applied to the control of an MES involving a cooling network shared by two facilities. The analysis of two summer days shows the benefits of the operating-point-dependent modeling of compression chillers. In accordance with renewable power generation as part of the electric power import, flexibility is provided by an ice storage unit and shiftable cooling demand. Case 2 addresses the planning of an MES. The object-oriented approach provides the framework to analyze different unit sizes and their optimal placement. Renewable power is generated locally by photovoltaics (PV) and it is imported from the main grid.

The electric power import covers renewable power from wind energy conversion systems (WECS) and PV, and power from fossil-fueled power stations. The output power of WECS and PV correlates with wind speed and solar irradiation. The output can be optimized by maximum power point tracking. Optimal and energy-efficient controls of WECS are widely discussed in the literature, e.g. in [25], [26]. With regard to the power point tracking of PV, relevant strategies may be found in [27]–[29].

For both study cases 1 and 2, the object-oriented modeling framework is implemented in MATLAB. The Gurobi optimizer [30] is used to solve the optimization problem.

A. Case 1: Operations Control for Reducing Cost of Cooling in MES

The first application case addresses the control of an MES involving a shared cooling network of a supermarket and an adjacent research building. The supermarket contributes an ice storage unit, whereas the research building provides shiftable cooling demand. The cooling demand of both facilities differs widely. As food refrigeration is essential at all times, the cooling demand of the supermarket is characterized by a base load, which is slightly higher during opening hours. By contrast, the cooling demand of the research building is caused by air conditioning and process cooling. Process cooling occurs mostly on working days between 07:00 h and 19:00 h. Thus, the cooling demand is dependent on the ambient temperature, the day of the week, and the time of the day.

Emphasizing the importance of modeling of power conversion units with operating-point-dependent efficiencies, two scenarios are studied. In scenario (a), the chillers are modeled with a constant conversion efficiency for cooling and ice production, respectively. Scenario (b) considers performance curves for the chillers that are dependent on cooling demand, ambient temperature, and operating mode as shown in Fig. 3.

1) Application of Object-oriented Modeling

The elements of the cooling network are modeled as presented in Sections II and III. Fig. 4 shows the object structure. The operation parameters of the resources are presented in Table III. Chiller 1 is an object of class "SIDO conversion" and therefore able to both produce cooling power and to charge the ice storage unit, as described in Section III. The other chillers are objects of class "SISO conversion" and solely produce cooling power. As the combined nominal cooling power of chillers 2, 3, and 4 is sufficient to cover the total cooling demand, chiller 1 may exclusively charge the ice storage unit. The ice storage unit is an object of class "Dual carrier storage". Shiftable cooling demand is an object of class "Prosumer". The shiftable cooling demand results from a research experiment that is typically planned to start at 07:00 h on working days. The experiment lasts for five hours and causes a constant cooling power demand of 40 kW. As the research experiment can be shifted by up to four hours, the latest possible start is at 11:00 h. Supermarket and research building are connected by a pipe represented by a cooling branch $\mathrm{Br}_{1,\mathrm{c}}$. The transfer efficiency $\eta_{\mathrm{Br1,c}}$ of the branch is 0.95.

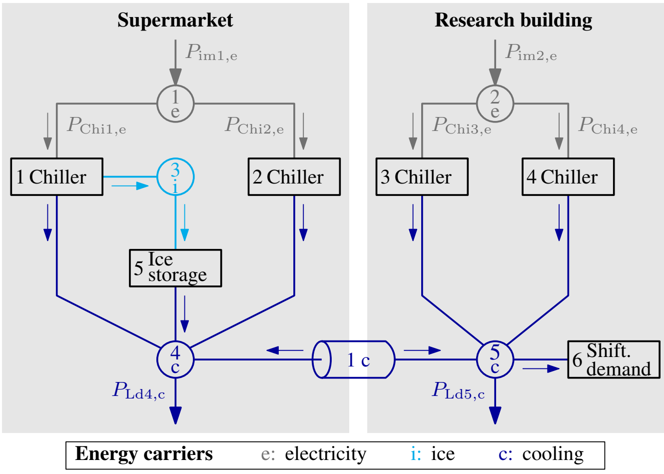

Fig. 4. Case 1: Object structure.

TABLE III
CASE 1: PARAMETERS OF RESOURCES

Object identifier	Class	Operation parameters
1 Chiller	SIDO conversion	$P^{\mathrm{nom}}_{\mathrm{Chi1,c}} = 80$ kW, $\eta^{\mathrm{nom}}_{\mathrm{Chi1,c}} = 4.0$ $P^{\mathrm{nom}}_{\mathrm{Chi1,i}} = 55$ kW, $\eta^{\mathrm{nom}}_{\mathrm{Chi1,i}} = 3.0$
2 Chiller	SISO conversion	$P^{\mathrm{nom}}_{\mathrm{Chi2,c}} = 80$ kW, $\eta^{\mathrm{nom}}_{\mathrm{Chi2,c}} = 4.0$
3 Chiller		$P^{\mathrm{nom}}_{\mathrm{Chi3,c}} = 40$ kW, $\eta^{\mathrm{nom}}_{\mathrm{Chi3,c}} = 4.0$
4 Chiller		$P^{\mathrm{nom}}_{\mathrm{Chi4,c}} = 140$ kW, $\eta^{\mathrm{nom}}_{\mathrm{Chi4,c}} = 4.0$
5 Ice storage	Dual carrier storage	$E^{\max}_{\mathrm{ISto}} = 1.0$ MWh, $P^{\max}_{\mathrm{ISto,c}} = 250$ kW, $P^{\max}_{\mathrm{ISto,i}} = 250$ kW, $\eta_{\mathrm{ISto,cha}} = 0.99$, $\eta_{\mathrm{ISto,dis}} = 0.99$, $\eta_{\mathrm{ISto,sd}} = 0.985$
6 Shiftable demand	Prosumer	$t_o = $ 07:00 h, $\Delta t_s = 4$ h

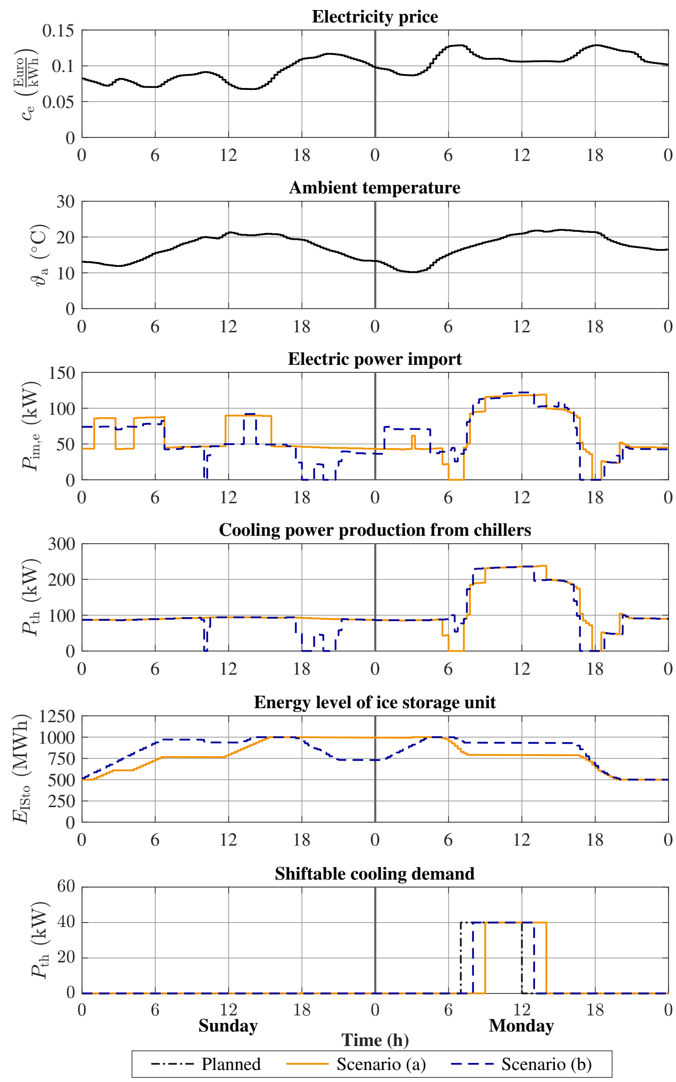

Fig. 5. Case 1: Cooling power supply of supermarket and research building including ice storage unit and shiftable cooling demand for two summer days. Scenario (a) with constant efficiencies, Scenario (b) with operating-point-dependent efficiencies for chillers.

The sum of input power $P_{\mathrm{Chi1,e}}$ and $P_{\mathrm{Chi2,e}}$ of chillers 1 and 2 determines the value of power import $P_{\mathrm{im1,e}}$ of node $\mathrm{No}_{1,\mathrm{e}}$. Therefore, the power balance of $\mathrm{No}_{1,\mathrm{e}}$ results in:

$$P_{\mathrm{im1,e}}(t_n) - P_{\mathrm{Chi1,e}}(t_n) - P_{\mathrm{Chi2,e}}(t_n) = 0 \tag{9}$$

Analogously, the value of power import $P_{\mathrm{im2,e}}$ of node $\mathrm{No}_{2,\mathrm{e}}$ is given by the sum of input power $P_{\mathrm{Chi3,e}}$ and $P_{\mathrm{Chi4,e}}$ of chillers 3 and 4. The power balance of $\mathrm{No}_{2,\mathrm{e}}$ is:

$$P_{\mathrm{im2,e}}(t_n) - P_{\mathrm{Chi3,e}}(t_n) - P_{\mathrm{Chi4,e}}(t_n) = 0 \tag{10}$$

The objective is to minimize the electricity costs for the cooling supply. The costs are determined by electric power import $P_{\mathrm{im1,e}}$ and $P_{\mathrm{im2,e}}$ as well as by the electricity price. The electricity price consists of constant levies and grid charges as well as of a flexible surcharge and the day-ahead energy price as introduced in [31]. The flexible surcharge and the day-ahead energy price depend on renewable power generation.

2) Optimization Results

As the spread between daily minimum and maximum temperatures is higher in summer, two consecutive summer days are analyzed. The results for both scenarios are presented in Fig. 5. In both scenarios, ice storage unit and shiftable cooling demand are utilized to decrease the electric power import in times of a high electricity price c_{e}. For example, c_{e} is comparatively low on Sunday from 01:00 h to 02:30 h, from 04:15 h to 06:30 h, and from 11:45 h to 15:15 h. A comparatively high c_{e} appears on Monday from 05:30 h to 07:30 h and from 17:00 h to 19:45 h. The ambient temperature ϑ_{a} is low on Sunday from 0:00 h to 04:30 h and on Monday from 00:45 h to 04:15 h.

In contrast to scenario (a) with constant chiller efficiencies, in scenario (b) the chillers are modeled with performance curves depending on the ambient temperature. As presented in Section III, the chillers operate more efficiently at low ambient temperatures. Therefore, in scenario (b) the combination of ambient temperature and electricity price affects the utilization of the chillers, whereas in scenario (a) the utilization of the chillers is only affected by the electricity price.

In scenario (a) the ice storage unit is charged during the three above mentioned time periods of low c_{e} on Sunday. By contrast, in scenario (b) the ice storage unit is charged on

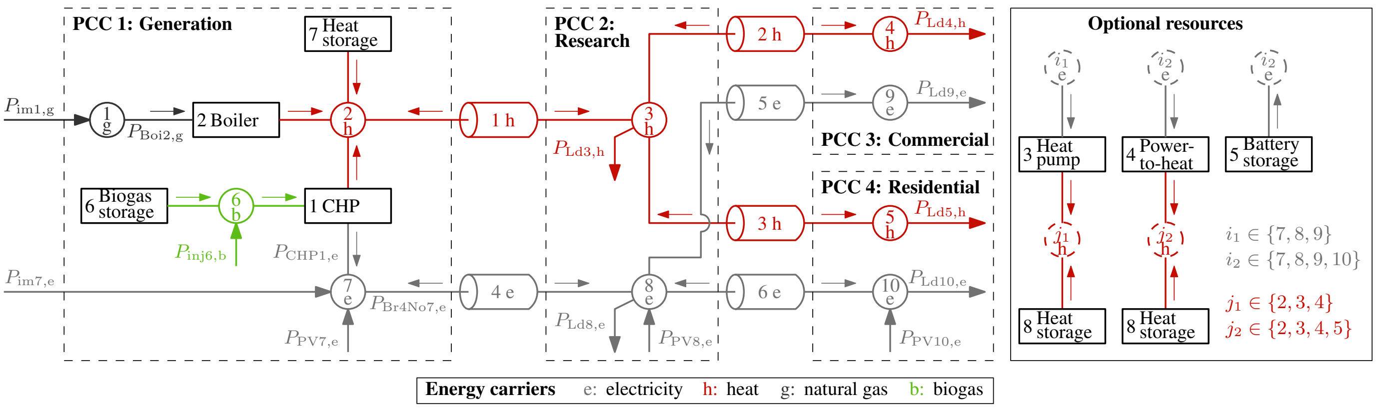

Fig. 6. Case 2: Object structure.

Sunday from 0:00 h to 06:30 h and from 13:15 h to 14:00 h, as well as on Monday from 0:45 h to 04:15 h. In all those intervals, the benefit comes from a combination of low ϑ_a and comparatively low c_e. Differences between the two scenarios also occur at discharging. As expected, in scenario (a), the ice storage unit is discharged during both mentioned time periods of high c_e on Monday. In scenario (b), the ice storage unit is also discharged on Sunday from 17:30 h to 21:00 h where a comparatively high c_e coincides with a comparatively high ϑ_a. The start of the shiftable cooling demand is shifted to 08:00 h in scenario (b) and to 09:00 h in scenario (a). This is due to the fact that the combination of c_e and ϑ_a is more beneficial for an earlier start of the shiftable demand. The results underline the importance of including operating-point-dependent efficiencies when performing operational control of an MES.

B. Case 2: Resource Planning for Reducing Primary Energy Usage in MES

The proposed object-oriented modeling framework is applied to the planning of resources of a technology campus. Within the MES, local photovoltaics and a biogas plant provide renewable energy. The biogas plant supplies a CHP unit producing heat and electricity. In addition, natural gas for a gas boiler and electricity are imported to fulfill the electricity and heat demand of the MES. In times of high renewable power generation, surplus electric power is exported. In times of high power demand and low renewable power generation, natural gas and electricity are imported. The campus management pursues the goal to decrease its dependence on primary energy. For this purpose, the installation of an additional resource providing flexibility is considered. For calculating the primary energy demand, primary energy factors according to [32] and [33] are used. The primary energy factor for electricity import is 1.8, for natural gas it is 1.1, for biogas it equals 0.5, and for electricity production from PV it is zero.

The MES is illustrated in Fig. 6. Within the MES, four points of common coupling (PCC) that are connected by an electricity and district heating network are considered. While generation units are connected to PCC 1, PCC 2 connects research facilities, PCC 3 connects commercial buildings, and PCC 4 connects households. Local PV is allocated to three of the four PCCs.

To achieve the goal of primary energy reduction, three options for additional resources are studied. Optional resources are a heat pump combined with a heat storage, a power-to-heat (P2H) unit combined with a heat storage, and a battery storage. With the exception of the heat pump, the resources are analyzed for all PCCs. The heat pump uses waste heat which is available at PCC 1, 2, and 3.

1) Application of Object-oriented Modeling

Figure 6 shows the object structure representing the described MES. Electric power import is represented by $P_{\mathrm{im7,e}}$ which is directly assigned to $\mathrm{No}_{7,\mathrm{e}}$. Natural gas import $P_{\mathrm{im1,g}}$ is directly assigned to $\mathrm{No}_{1,\mathrm{g}}$. The injection of biogas flow $P_{\mathrm{inj6,b}}$ is given by a profile and directly assigned to $\mathrm{No}_{6,\mathrm{b}}$. The electricity and district heating networks are represented by four electricity nodes, four heat nodes, three electricity branches, and three heat branches. For each PCC, there is one heat node and one electricity node where the loads and uncontrollable power generation from PV are allocated. The electric power demand is generated using characteristic standard load profiles, depending on seasons and weekdays. The heat demand is dependent on ambient temperature, time of day, and user characteristics. The PV power generation profile is taken from a real PV plant in Berlin-Adlershof. The characteristics of uncontrollable generation and demand are summarized for the respective nodes in Table IV. Electricity and heat branches connect the nodes. The branch parameters of maximum power transfer and transfer efficiency depend on the length of pipes and lines and are given in Table V. Table VI contains operation parameters of conversion resources. The CHP is an object of class "SIDO conversion" with a biogas input node, a heat output node and an electricity output node. As the biogas boiler as well as the optional heat pump and P2H each have one input and one output, they are objects of class "SISO conversion". Information about storage resources is summarized in Table VII. All four considered storage units are objects of class "Single carrier storage".

The natural gas input of the boiler $P_{\mathrm{Boi2,g}}$ determines the value of $P_{\mathrm{im1,g}}$ at $\mathrm{No}_{1,\mathrm{g}}$. Analogously, $P_{\mathrm{im7,e}}$ at $\mathrm{No}_{7,\mathrm{e}}$ is determined by PV generation $P_{\mathrm{PV7,e}}$, electric output power from CHP $P_{\mathrm{CHP1,e}}$ and power over the electric branch $P_{\mathrm{Br4No7,e}}$. For both nodes, the power balances result in:

$$P_{\mathrm{im1,g}}(t_n) - P_{\mathrm{Boi2,g}}(t_n) = 0 \qquad (11)$$

$$P_{\mathrm{im7,e}}(t_n) + P_{\mathrm{PV7,e}}(t_n) + P_{\mathrm{CHP1,e}}(t_n) + P_{\mathrm{Br4No7,e}}(t_n) = 0 \qquad (12)$$

TABLE IV
CASE 2: CHARACTERISTICS OF UNCONTROLLABLE NODAL INJECTION

Node	Yearly demand	Yearly generation
$\mathrm{No}_{1,\mathrm{g}}$	–	–
$\mathrm{No}_{2,\mathrm{h}}$	–	–
$\mathrm{No}_{3,\mathrm{h}}$	1,000 MWh	–
$\mathrm{No}_{4,\mathrm{h}}$	400 MWh	–
$\mathrm{No}_{5,\mathrm{h}}$	1,500 MWh	–
$\mathrm{No}_{6,\mathrm{b}}$	–	2,750 MWh
$\mathrm{No}_{7,\mathrm{e}}$	–	250 MWh
$\mathrm{No}_{8,\mathrm{e}}$	1,500 MWh	400 MWh
$\mathrm{No}_{9,\mathrm{e}}$	600 MWh	–
$\mathrm{No}_{10,\mathrm{e}}$	800 MWh	400 MWh

TABLE V
CASE 2: PARAMETERS OF BRANCHES

Branch	Maximum power transfer $P^{\max}_{\mathrm{Br}k,\alpha}$	Transfer efficiency $\eta_{\mathrm{Br}k,\alpha}$
$\mathrm{Br}_{1,\mathrm{h}}$	1,500 kW	0.95
$\mathrm{Br}_{2,\mathrm{h}}$	300 kW	0.95
$\mathrm{Br}_{3,\mathrm{h}}$	800 kW	0.9
$\mathrm{Br}_{4,\mathrm{e}}$	3,000 kW	0.98
$\mathrm{Br}_{5,\mathrm{e}}$	1,000 kW	0.99
$\mathrm{Br}_{6,\mathrm{e}}$	1,000 kW	0.98

TABLE VI
CASE 2: PARAMETERS OF CONVERSION RESOURCES

Object identifier	Class	Operation parameters	
		Power limits	Conversion efficiencies
1 CHP	SIDO conversion	$P^{\max}_{\mathrm{CHP,h}} = 250$ kW $P^{\max}_{\mathrm{CHP,e}} = 150$ kW	$\eta_{\mathrm{CHP,h}} = 0.55$ $\eta_{\mathrm{CHP,e}} = 0.33$
2 Boiler	SISO conversion	$P^{\max}_{\mathrm{Boi,h}} = 1{,}200$ kW	$\eta_{\mathrm{Boi,h}} = 0.9$
3 Heat pump		scenario specific	$\eta_{\mathrm{HeP,h}} = 3.0$
4 P2H		scenario specific	$\eta_{\mathrm{P2H,h}} = 0.98$

TABLE VII
CASE 2: PARAMETERS OF STORAGE RESOURCES

Object identifier	Class	Operation parameters			
		$E^{\max}_{\mathrm{Sto}}$	$P^{\max}_{\mathrm{Sto}}$	$\eta_{\mathrm{cha}}, \eta_{\mathrm{dis}}$	η_{sd}
5 Battery storage	Single carrier storage	scenario specific	200 kW	0.95	0.999
6 Biogas storage		10.0 MWh	1,000 kW	0.99	0.997
7 Heat storage		5.0 MWh	1,000 kW	0.99	0.975
8 Heat storage		2.0 MWh	500 kW	0.99	0.975

In the optimization, the primary energy demand is reduced by allocating electricity and gas prices to imported energy, affiliated with $P_{\mathrm{im7,e}}$ and $P_{\mathrm{im1,g}}$. Then, the costs are minimized. As in use case 1, the electricity price consists of constant levies and grid charges as well as of a flexible surcharge and the day-ahead energy price as introduced in [31]. The gas price is assumed to be constant.

Thanks to the usage of nodes as coupling elements in the modeling approach, only the power balances at the nodes where the optional resources would be placed are affected by an expansion. For example, if the location of the heat pump is changed from $\mathrm{No}_{2,\mathrm{h}}$ to $\mathrm{No}_{3,\mathrm{h}}$, only the allocations at the heat pump object and at both nodes are updated. For changing the size of an optional unit, the specific operation parameter is adapted.

2) *Optimization Results*

The analysis is performed for the three years of 2016, 2017, and 2018. Fig. 7 shows the calculated yearly primary energy reduction for the different sizes and locations of the optional resources. The highest reduction is achieved by a heat pump with a maximum heat power of 300 kW combined with a heat storage of 2 MWh located at PCC 2. Depending on the studied year, a primary energy reduction from 255 MWh/a to 270 MWh/a is attained in this case. The reduction potential of a heat pump with a heat power of 200 kW is still superior to the best result obtained with a P2H unit. The most effective installation of the P2H unit is achieved at PCC 4. Here, the primary energy demand is reduced by up to 185 MWh/a with a P2H unit of 500 kW and a heat storage of 2 MWh. The highest reduction that is achieved by a battery storage amounts to 140 MWh/a with a storage capacity of 2 MWh located at PCC 2.

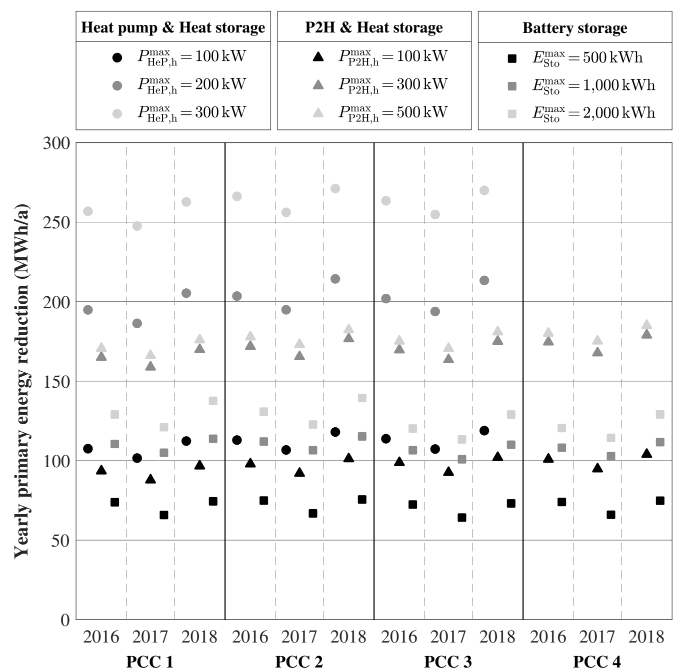

Fig. 7. Case 2: Calculated yearly primary energy reduction for different sizes and locations of optional resources and for the years 2016, 2017, and 2018.

The installation of a heat pump combined with a heat storage is by far the best option in this study case. This is due to the fact that heat pumps convert electricity to heat very efficiently assuming the availability of waste heat as required. Therefore, the electricity from local PV or from the biogas CHP that is not used to satisfy the electricity demand can be converted to heat and replace heat generation from natural gas. The best location for heat pumps and battery storage is PCC 2 since PCC 2 is in the center of the MES and transfer losses to other PCCs are low. Due to the comparatively large amount of renewable energy from PV and the high heat demand, PCC 4 is the best location for the P2H unit. Here, the surplus electric energy can be directly converted to heat.

V. Conclusion

An object-oriented modeling framework for planning and control of multi-energy systems was developed, implemented, and validated. This resulted in three main contributions. First, the modeling framework provides base classes representing a multi-energy system. Thanks to the applied abstraction, classes are formulated independent of specific energy carriers. The classes are formed with regard to common attributes and functions of network elements. This also applies to the nodes. The nodes serve as coupling elements that facilitate the modeling of arbitrary topologies.

Second, the definition of the class operations is flexible taking into account the situation. Depending on the situation, the class operations can be formulated at different levels of detail. This is essential for the modeling of network elements in response to the desired levels of accuracy.

Third, the object-oriented modeling framework lends itself to the application of planning on the one hand and to the application of operations control on the other hand. The application of planning takes advantage of the abstraction of formulating network elements independent of specific energy carriers. This facilitates the analysis of different resource options in the planning of multi-energy systems. The final selection of the energy carrier could then be made by an optimizer. Furthermore, the flexibility of the class operations supports the adaption to the applications of interest to the user. For planning applications, the class operations may be formulated in a compact way to reduce computational effort. For operations control, a more detailed description of the class operations can be made readily available.

The modeling framework was applied to the resource planning of a technology campus. Furthermore, the importance of flexible class operations was shown in an application of operations control, putting into evidence the value of considering efficiencies as a function of operating points. The study cases have confirmed the validity of the object-oriented modeling framework and its versatility with respect to application. As such, the modeling framework can provide the basis for a wide variety of additional energy management systems that are valuable for the development of the energy internet.

References

[1] G. Chicco and P. Mancarella, "Distributed multi-generation: A comprehensive view," *Renewable and Sustainable Energy Reviews*, vol. 13, no. 3, pp. 535–551, Apr. 2009.

[2] R. F. Zhang, T. Jiang, G. Q. Li, H. H. Chen, X. Li, L. Q. Bai, and H. T. Cui, "Day- ahead scheduling of multi-carrier energy systems with multi-type energy storages and wind power," *CSEE Journal of Power and Energy Systems*, vol. 4, no. 3, pp. 283–292, Sep. 2018.

[3] Q. Fu, A. Hamidi, A. Nasiri, V. Bhavaraju, S. B. Krstic, and P. Theisen, "The role of energy storage in a microgrid concept: Examining the opportunities and promise of microgrids," *IEEE Electrification Magazine*, vol. 1, no. 2, pp. 21–29, Dec. 2013.

[4] A. Bischi, L. Taccari, E. Martelli, E. Amaldi, G. Manzolini, P. Silva, S. Campanari, and E. Macchi, "A detailed MILP optimization model for combined cooling, heat and power system operation planning," *Energy*, vol. 74, pp. 12–26, Sep. 2014.

[5] M. Ameri and Z. Besharati, "Optimal design and operation of district heating and cooling networks with CCHP systems in a residential complex," *Energy and Buildings*, vol. 110, pp. 135–148, Jan. 2016.

[6] Z. M. Li and Y. Xu, "Optimal coordinated energy dispatch of a multi-energy microgrid in grid-connected and islanded modes," *Applied Energy*, vol. 210, pp. 974–986, Jan. 2018.

[7] M. Geidl and G. Andersson, "Operational and topological optimization of multi-carrier energy systems," in *2005 International Conference on Future Power Systems*, 2005, pp. 1–6.

[8] M. Geidl and G. Andersson, "Optimal power flow of multiple energy carriers," *IEEE Transactions on Power Systems*, vol. 22, no. 1, pp. 145–155, Feb. 2007.

[9] A. Maroufmashat, A. Elkamel, M. Fowler, S. Sattari, R. Roshandel, A. Hajimiragha, S. Walker, and E. Entchev, "Modeling and optimization of a network of energy hubs to improve economic and emission considerations," *Energy*, vol. 93, pp. 2546–2558, Dec. 2015.

[10] X. P. Zhang, L. Che, M. Shahidehpour, A. S. Alabdulwahab, and A. Abusorrah, "Reliability-based optimal planning of electricity and natural gas interconnections for multiple energy hubs," *IEEE Transactions on Smart Grid*, vol. 8, no. 4, pp. 1658–1667, Jul. 2017.

[11] G. Chicco and P. Mancarella, "Matrix modelling of small-scale trigeneration systems and application to operational optimization," *Energy*, vol. 34, no. 3, pp. 261–273, Mar. 2009.

[12] Y. Wang, N. Zhang, C. Q. Kang, D. S. Kirschen, J. W. Yang, and Q. Xia, "Standardized matrix modeling of multiple energy systems," *IEEE Transactions on Smart Grid*, vol. 10, no. 1, pp. 257–270, Jan. 2019.

[13] W. J. Huang, N. Zhang, J. W. Yang, Y. Wang, and C. Q. Kang, "Optimal configuration planning of multi-energy systems considering distributed renewable energy," *IEEE Transactions on Smart Grid*, vol. 10, no. 2, pp. 1452–1464, Mar. 2019.

[14] T. F. Ma, J. Y. Wu, and L. L. Hao, "Energy flow modeling and optimal operation analysis of the micro energy grid based on energy hub," *Energy Conversion and Management*, vol. 133, pp. 292–306, Feb. 2017.

[15] S. Long, O. Marjanovic, and A. Parisio, "Generalised control-oriented modelling framework for multi-energy systems," *Applied Energy*, vol. 235, pp. 320–331, Feb. 2019.

[16] G. Booch, *Object-Oriented Analysis and Design with Applications*, 2nd ed. Redwood City, California: The Benjamin/Cummings Publishing Company, Inc., 1994.

[17] İ. Dinçer, *Refrigeration Systems and Applications*, 3rd ed. Chichester, West Sussex, United Kingdom: John Wiley & Sons, 2017.

[18] S. Bschorer, M. Kuschke, and K. Strunz, "Cost ratio analysis evaluating the potential of an ice storage unit in a multi-energy microgrid," in *2017 IEEE PES Innovative Smart Grid Technologies Conference Europe*, 2017, pp. 1–6.

[19] P. Sreedharan and P. Haves, "Comparison of chiller models for use in model-based fault detection," in *International Conference for Enhanced Building Operations*, 2001, pp. 1–10.

[20] M. Hydeman and K. L. Gillespie, "Tools and techniques to calibrate electric chiller component models," *ASHRAE Transactions*, vol. 108, no. 1, pp. 733–741, 2002.

[21] P. S. Mark Hydeman, N. Webb, and S. Blanc, "Development and testing of a reformulated regression-based electric chiller model," *ASHRAE Transactions*, vol. 108, no. 2, pp. 1118–1127, 2002.

[22] TRANE, "Air-Cooled Series R^{TM} Helical-Rotary Liquid Chiller," TRANE, Belgium, Model RTAC 120 to 400, 2010.

[23] İ. Dinçer and M. A. Rosen, *Thermal Energy Storage: Systems and Applications,* 2nd ed., Chichester, West Sussex, United Kingdom: John Wiley & Sons, 2011.

[24] Z. M. Zhu, J. Tang, S. Lambotharan, W. H. Chin, and Z. Fan, "An integer linear programming based optimization for home demand-side management in smart grid," in *2012 IEEE PES Innovative Smart Grid Technologies*, 2012, pp. 1–5.

[25] I. Munteanu, N. A. Cutululis, A. I. Bratcu, and E. Ceanga, *Optimal Control of Wind Energy Systems: Towards a Global Approach*. London: Springer, 2008.

[26] M. Kuschke and K. Strunz, "Energy-efficient dynamic drive control for wind power conversion with PMSG: Modeling and application of transfer function analysis," *IEEE Journal of Emerging and Selected Topics in Power Electronics*, vol. 2, no. 1, pp. 35–46, Mar. 2014.

[27] W. D. Xiao, *Photovoltaic Power System: Modeling, Design and Control*. Hoboken: John Wiley & Sons, 2017.

[28] M. Adly and K. Strunz, "Efficient digital control for MPP tracking and output voltage regulation of partially shaded PV modules in DC bus and DC microgrid systems," *IEEE Transactions on Power Electronics*, vol. 34, no. 7, pp. 6309–6319, Jul. 2019.

[29] B. Yang, L. E. Zhong, X. S. Zhang, H. C. Shu, T. Yu, H. F. Li, L. Jiang, and L. M. Sun, "Novel bio-inspired memetic salp swarm algorithm and application to MPPT for PV systems considering partial shading

condition," *Journal of Cleaner Production*, vol. 215, pp. 1203–1222, Apr. 2019.
[30] GUROBI Optimization, LLC. (2019). "GUROBI optimizer reference manual," 2019. [Online]. Available: http://www.gurobi.com
[31] S. Bschorer, M. Kuschke, and K. Strunz, "Analysis of the interdependence of carbon emissions savings and electricity tariffs for a business facility with an ice storage unit," in *International ETG Congress 2017*, 2017, pp. 1–6.
[32] German Federal Government, "Verordnung über energiesparenden Wärmeschutz und energiesparende Anlagentechnik bei Gebäuden (Energieeinsparverordnung – EnEV)," 2014.
[33] *Energy efficiency of buildings – calculation of the net, final and primary energy demand for heating, cooling, ventilation, domestic hot water and lighting*, DIN V 18599-2011, 2018.

Stefan Bschorer received the M.Sc. degree in Electrical Engineering and Information Technology from Technische Universität München (TUM), Munich, Germany, in 2014. He is currently pursuing his Ph.D. in Electrical Engineering at Technische Universität Berlin (TUB), Germany. His research interests include modeling and optimization of multi-energy systems with special focus on electricity and cooling networks.

Maren Kuschke received the Dipl.-Ing. and Dr.-Ing. degrees from Technische Universität Berlin (TUB), Germany, in 2008 and 2014, respectively. She studied electrical engineering with focus on electrical drives, photovoltaics, and electric energy systems at TU Berlin and KTH Stockholm, Sweden.

Maren Kuschke received the VDI Award from the Association of German Engineers in 2009 and the IEEE PES German Chapter Best Master Thesis Award in 2010. She is recipient of the IEEE PES Prize Paper Award 2015.

Kai Strunz received the Dipl.-Ing. and Dr.-Ing. (summa cum laude) degrees from Saarland University, Saarbrücken, Germany, in 1996 and 2001, respectively. From 1995 to 1997, he pursued research with Brunel University in London. From 1997 to 2002, he worked with the Division Recherche et Développement of Electricité de France in the Paris area. From 2002 to 2007, he was an Assistant Professor of electrical engineering with the University of Washington in Seattle. Since September 2007, he has been Professor with the Institute of Sustainable Electric Networks and Sources of Energy, Technische Universität Berlin, Germany. He has been a Guest Professor at the Institute of Electrical Engineering of the Chinese Academy of Sciences since 2017.

Dr. Strunz is the Chairman of the IEEE Power and Energy Society Subcommittee on Distributed Energy Resources. In 2012, he was the General and Technical Program Chair of the IEEE PES Innovative Smart Grid Technologies Europe 2012 in Berlin. He was the recipient of the IEEE PES Prize Paper Award in 2015 and the Journal of Emerging and Selected Topics in Power Electronics First Prize Paper Award 2015.